16 April 2010 | $10

Science

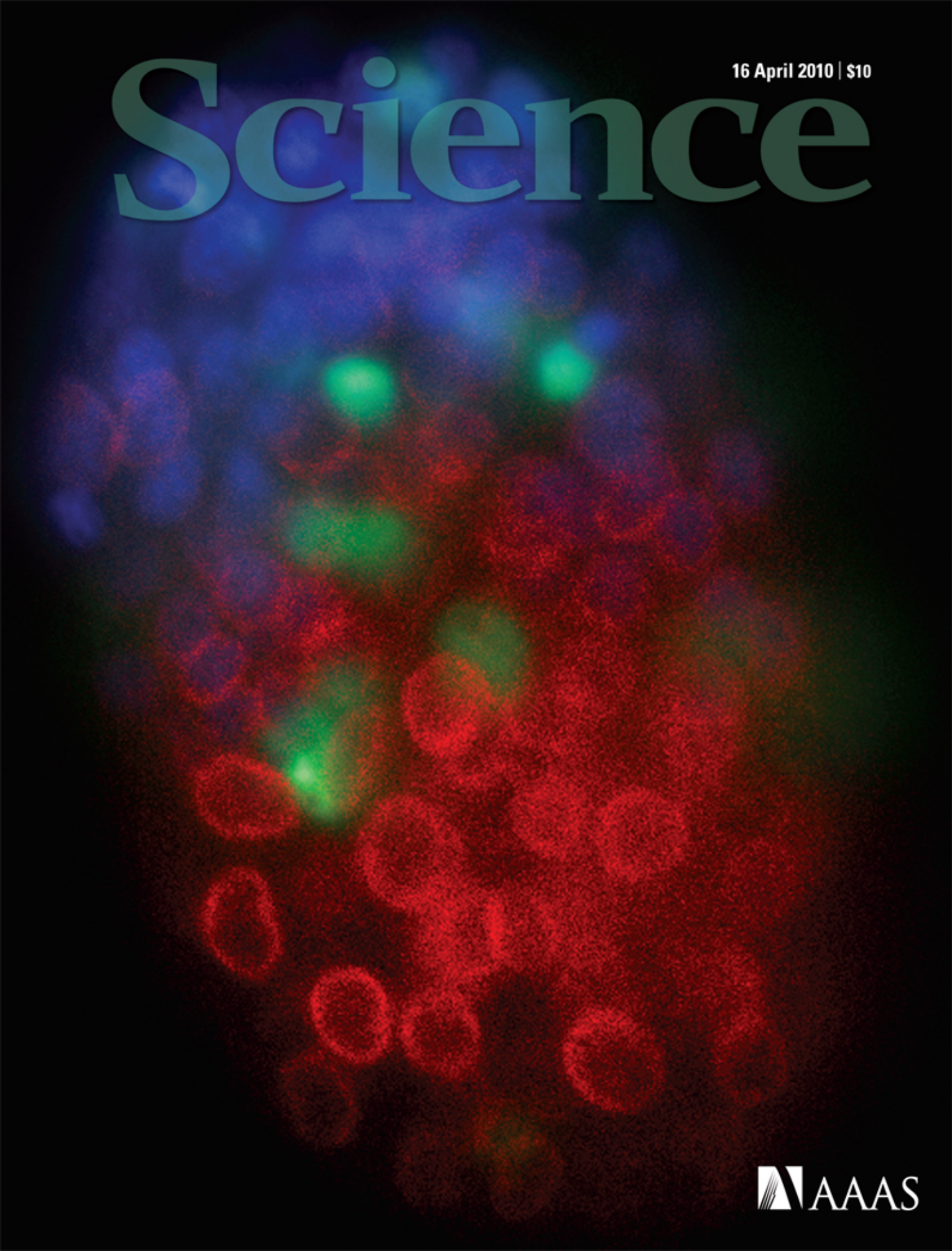

AAAS

Caspase-Dependent Conversion of Dicer Ribonuclease into a Death-Promoting Deoxyribonuclease

Akihisa Nakagawa,[1]* Yong Shi,[1]* Eriko Kage-Nakadai,[2] Shohei Mitani,[2] Ding Xue[1]†

Chromosome fragmentation is a hallmark of apoptosis, conserved in diverse organisms. In mammals, caspases activate apoptotic chromosome fragmentation by cleaving and inactivating an apoptotic nuclease inhibitor. We report that inactivation of the *Caenorhabditis elegans dcr-1* gene, which encodes the Dicer ribonuclease important for processing of small RNAs, compromises apoptosis and blocks apoptotic chromosome fragmentation. DCR-1 was cleaved by the CED-3 caspase to generate a C-terminal fragment with deoxyribonuclease activity, which produced 3′ hydroxyl DNA breaks on chromosomes and promoted apoptosis. Thus, caspase-mediated activation of apoptotic DNA degradation is conserved. DCR-1 functions in fragmenting chromosomal DNA during apoptosis, in addition to processing of small RNAs, and undergoes a protease-mediated conversion from a ribonuclease to a deoxyribonuclease.

One of the hallmarks of apoptosis is fragmentation of chromosomal DNA at internucleosomal regions, which generates DNA fragments differing by ~180 base pairs and contributes to the irreversible cell killing process (*1*, *2*). Multiple deoxyribonucleases (DNases) have been implicated in mediating apoptotic DNA fragmentation, including 40-kD DNA fragmentation factor (DFF40), also known as caspase-activated deoxyribonuclease (CAD); endonuclease G (endoG); deoxyribonuclease II (DNase II); and several other nucleases (*3*, *4*). DFF40 is a component of a DNA fragmentation factor complex, which also contains an inhibitory subunit, DFF45 (also known as ICAD, inhibitor of CAD) (*5*–*8*). DFF45 serves both as a chaperone for the proper folding of DFF40 and as a cognate inhibitor that holds DFF40 activity in check in normal cells. During apoptosis, the cleavage of DFF45 by activated caspases, such as caspase-3 and caspase-7, results in the release and activation of DFF40 (*5*–*8*). The activated DFF40 nuclease then associates with chromosomal proteins, such as histone H1, HMG (high-mobility group) proteins, and topoisomerase II, to promote cleavage of internucleosomal DNA, generating 3′ hydroxyl DNA breaks that can be detected by the TUNEL [terminal deoxynucleotidyl transferase (TdT)–mediated deoxyuridine triphosphate (dUTP) nick end labeling] assay (*6*, *9*, *10*). In mice deficient in either DFF40 or DFF45, which is needed for proper folding of DFF40, chromosome fragmentation fails to occur during apoptosis (*11*, *12*).

[1]Department of Molecular, Cellular, and Developmental Biology, University of Colorado, Boulder, CO 80309, USA. [2]Department of Physiology, Tokyo Women's Medical University, School of Medicine, and Core Research for Evolutional Science and Technology (CREST), Japan Science and Technology Agency, Tokyo 162-8666, Japan.

*These authors contributed equally to this work.
†To whom correspondence should be addressed. E-mail: ding.xue@colorado.edu

A mitochondrial nuclease, endoG, mediates residual apoptotic DNA fragmentation observed in DFF45-deficient cells (*13*). EndoG is released from mitochondria during apoptosis and translocates into the nucleus to facilitate chromosome fragmentation (*13*). EndoG is a member of a conserved family of endonucleases, including the *Caenorhabditis elegans* CPS-6 (CED-3 protease suppressor) nuclease (*14*, *15*). In *C. elegans* animals deficient in *cps-6*, TUNEL-stained nuclei accumulate in mutant embryos, and developmental cell death is delayed or even inhibited in sensitized genetic backgrounds, such as animals partially deficient for the CED-3 caspase (*14*), which suggests that CPS-6 is important for apoptotic DNA degradation and the progression of apoptosis. In addition to *cps-6*, seven cell death–related nucleases (named CRN nucleases) have been identified in a candidate-based RNA interference (RNAi) screen in *C. elegans* (*16*). RNAi-mediated depletion of six of these *crn* nuclease genes (*crn-1* to *crn-5* and *cyp-13*) results in similar cell death defects, including accumulation of TUNEL-stained nuclei in RNAi-treated embryos and inhibition of apoptosis in sensitized genetic backgrounds (*16*). Biochemical analysis reveals that some of these CRN nucleases interact with CPS-6 and with one another to promote step-wise DNA degradation, by first turning the 3′ OH DNA nicks into small gaps through their exonuclease activities and then creating double-stranded DNA (dsDNA) breaks via a gap-dependent endonuclease activity (*16*, *17*). Two *C. elegans* DNase II homologs, NUC-1 and CRN-6, function in a later stage to complete degradation of chromosomal DNA (*16*, *18*), as loss of either gene or both also results in accumulation of TUNEL-stained nuclei but does not affect the activation or the kinetics of apoptosis (*14*, *18*). In all instances, loss of any one or a combination of the nine *C. elegans* apoptotic nucleases results in accumulation of TUNEL-stained nuclei, which indicates that these nucleases function in resolving 3′ OH DNA breaks generated during apoptosis and that at least one additional *C. elegans* nuclease—presumably, a functional analog of DFF40—is activated during apoptosis to generate 3′ OH DNA breaks. Because no candidate DFF40 or DFF45 homolog is predicted to be encoded by the *C. elegans* genome (*4*), it remains enigmatic how apoptotic DNA degradation is initiated in *C. elegans*. We report that this role is played by the *C. elegans* Dicer ribonuclease.

Dicer is a highly conserved ribonuclease that plays a central role in processing double-stranded RNA (dsRNA) to generate small RNAs important for various gene-silencing events (*19*–*26*). It is an RNase III enzyme that processes precursor dsRNA into small duplex RNA species of about 21 to 25 nucleotides, with 5′ phosphate and 3′ hydroxyl termini (*22*, *27*–*30*). These small RNAs are then unwound and incorporated into various silencing complexes, such as the RNA-induced silencing complex (RISC), that direct sequence-specific cleavage or translational repression of complementary mRNA (*24*–*26*, *31*–*34*). Multiple proteins have been identified to serve as Dicer cofactors or interactors to mediate various gene silencing events, including proteins in the Argonaute family that contain PAZ (Piwi, Argo, and Zwille) and PIWI domains (*32*–*34*); RDE-1 (RNAi defective, also an Argonaute protein); RDE-4 and its fly homolog R2D2; DRH-1 and DRH-2 (Dicer-related helicases) (*31*, *35*, *36*); ERI-1 (enhanced RNAi); and RRF-3 (RNA-dependent RNA polymerase family) (*26*, *37*, *38*). Dicer enzymes typically contain a DExH-box helicase domain (*39*), a PAZ domain, two tandem RNase III domains (RNase IIIa and IIIb), and a dsRNA binding domain (*40*, *41*). The intramolecular dimerization of the two RNase III domains of Dicer generates the dicing activity (*29*), and the distance between the PAZ and RNase III domains determines the length of small RNA fragments processed (*42*). Dicer is important for multiple cellular processes, including viral defense, chromatin remodeling, genome rearrangement, developmental timing, and stem cell maintenance (*21*, *23*, *43*–*48*). These cellular functions likely are attributed to the generation of small interfering RNAs (siRNAs), microRNAs (miRNAs), and other small RNAs (*34*, *41*). We uncovered a previously uncharacterized role of *C. elegans* Dicer (DCR-1) in activating the apoptotic DNA degradation process that is dependent on generation of a new DNase activity through cleavage by the cell death protease CED-3 and that is independent of Dicer's actions in gene silencing in *C. elegans*.

***dcr-1* is required for initiating apoptotic DNA degradation in *C. elegans*.** To identify nucleases that function in apoptotic DNA degradation in *C. elegans* and, in particular, nucleases that generate 3′ hydroxyl DNA breaks during apoptosis, we performed RNAi on *cps-6(sm116)* mutant animals, which contain an average of 16 TUNEL-stained cells in early-stage embryos

(Fig. 1, A and B), and looked for RNAi knockdown of nucleases that reduced the number of TUNEL-stained cells in *cps-6(sm116)* embryos (*16*, *17*, *49*). We found that *dcr-1* RNAi reduced the number of TUNEL signals in *cps-6(sm116)* embryos (Fig. 1A). Given that *dcr-1* RNAi also reduces the efficiency of RNA interference, we examined whether two deletion mutations in *dcr-1* (*ok247* and *pk1351*) caused a stronger reduction in TUNEL staining in the *cps-6(sm116)* mutant. Because *dcr-1* loss-of-function (*lf*) mutants are sterile, a balancer, *hT2(qIs48)*, was used to maintain the *dcr-1(lf)* heterozygous strain. *qIs48* is a transgene integrated into the *hT2* chromosome and carries a $P_{myo\text{-}2}gfp$ reporter that directs strong green fluorescent protein (GFP) expression in the pharynx in most developmental stages. *dcr-1(lf)* homozygous embryos derived from the *dcr-1(lf)/hT2* mother can thus be identified as embryos that do not express GFP. We performed TUNEL and anti-GFP double staining to score the number of TUNEL-stained cells in *dcr-1(lf)* embryos (*49*). Although *dcr-1(ok247)* and *dcr-1(pk1351)* homozygous embryos had comparable numbers of TUNEL-stained cells to those seen in *dcr-1(ok247)/hT2* and *dcr-1(pk1351)/hT2* heterozygous embryos or wild-type N2 embryos

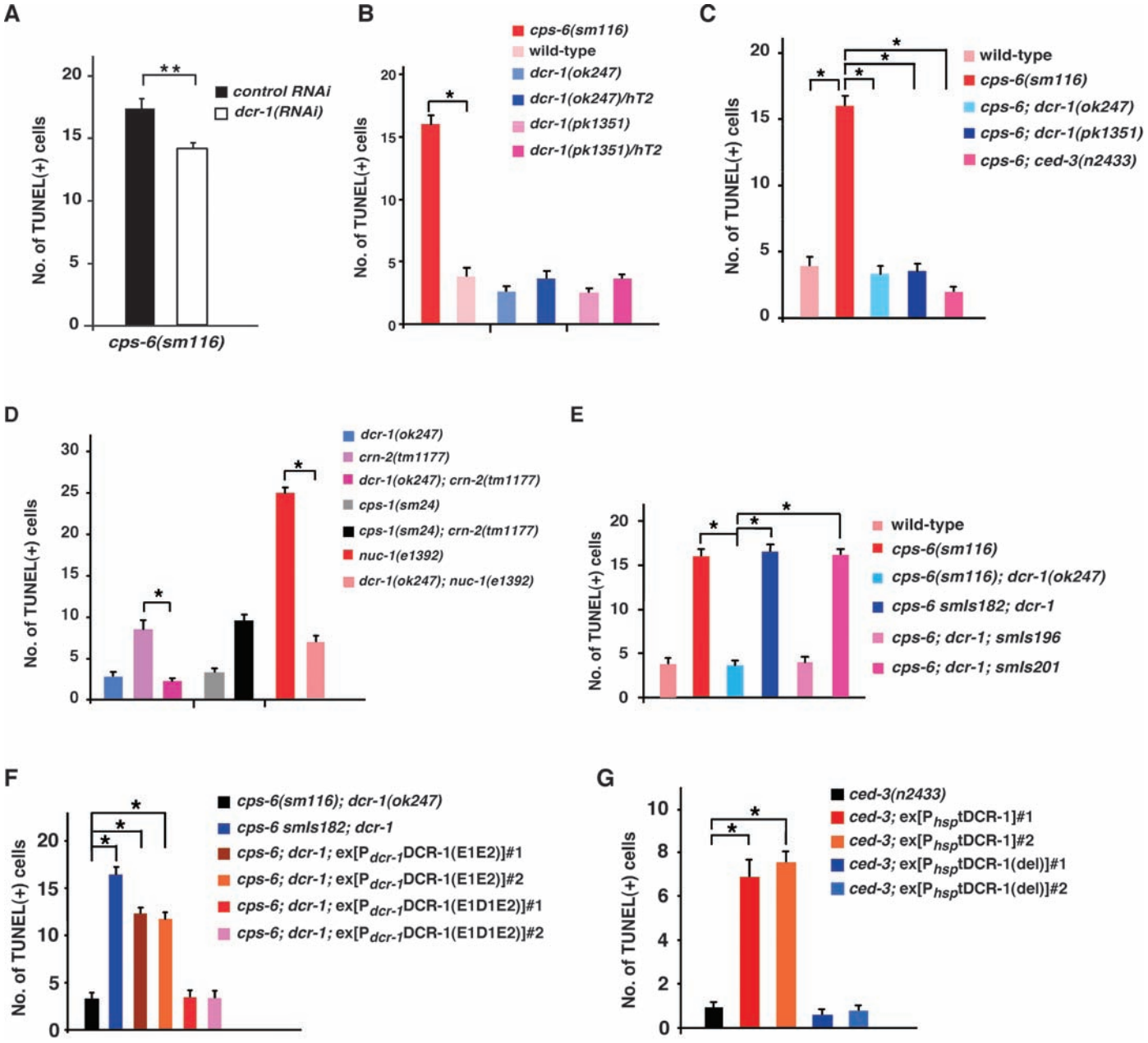

Fig. 1. Role of DCR-1 in creating TUNEL-reactive DNA breaks in apoptotic cells. (**A** to **G**) TUNEL staining was monitored in the indicated strains (*49*). In most cases, GFP-specific immunostaining and TUNEL staining were done to quantify the number of TUNEL-stained cells in *dcr-1(lf)* homozygous embryos (*49*), which were identified as embryos lacking GFP derived from *dcr-1(lf)/hT2(qIs48)* mothers. In animals carrying $P_{sur\text{-}5}sur\text{-}5::gfp$ as a transgenic marker (E and F), *dcr-1(lf)* homozygous transgenic embryos were identified as embryos with nuclear GFP expression in many cells but lacking pharyngeal GFP expression (*qIs48*). RNAi experiments were done as described (*14*). All *cps-6(sm116)* strains also contain *dpy-5(e61)*. *smIs182* is an integrated transgene carrying $P_{dcr\text{-}1}$DCR-1. *smIs196* is an integrated transgene carrying $P_{dcr\text{-}1}$DCR-1(D1742E). *smIs201* is an integrated transgene carrying $P_{dcr\text{-}1}$tDCR-1. Each numbered array represents an independent transgenic line (F and G). The *y* axis represents average number of TUNEL-stained cells scored, and error bars represent SEM. For each strain, 15 comma-stage embryos were scored. The significance of differences between different strains was determined by unpaired *t* test (A) or one-way analysis of variance (ANOVA), followed by Tukey's test (B) to (G). $*P < 0.001$; $**P < 0.05$.

(Fig. 1B), both *dcr-1(ok247)* and *dcr-1(pk1351)* deletion mutations reduced the number of TUNEL signals in *cps-6(sm116)* embryos to that seen in wild-type embryos (Fig. 1C). These findings suggested that *dcr-1* does function in generating TUNEL-reactive DNA breaks that fail to be resolved in *cps-6(sm116)* embryos. Similarly, *dcr-1(ok247)* significantly reduced the number of TUNEL signals in *crn-2(tm1177)* embryos, which are defective in another apoptotic nuclease CRN-2 (Fig. 1D) (*16*). *dcr-1(ok247)* also reduced the number of TUNEL-stained cells in *nuc-1(e1392)* embryos (Fig. 1D). Taken together, these results indicate that DCR-1 functions in creating TUNEL-reactive DNA breaks in apoptotic cells that are later resolved by other apoptotic nucleases, such as CPS-6, CRN-2, and NUC-1, and that *dcr-1* likely acts upstream of *cps-6*, *crn-2*, and *nuc-1* to promote apoptotic DNA degradation.

***dcr-1* promotes apoptosis.** We next investigated whether *dcr-1* affects programmed cell death in *C. elegans*. We examined the appearance of apoptotic cell corpses in developing embryos, which is a sensitive assay for detecting weak cell-death defects (*14*, *16*, *50*). We observed significantly fewer cell corpses in both *dcr-1(ok247)* and *dcr-1(pk1351)* mutants at most embryonic stages than in wild-type embryos (Fig. 2A). Thus, *dcr-1* appears to be a proapoptotic factor. The cell-death defect displayed by the *dcr-1(lf)* mutants is stronger than that observed in the *cps-6(sm116)* mutant or animals deficient in most *crn* genes, in which cell death in developing embryos is delayed rather than reduced (*14*, *16*). Moreover, both *dcr-1(ok247)* and *dcr-1(pk1351)* mutations reduced the number of persistent cell corpses in *ced-1(e1735)* embryos, in which engulfment of cell corpses is blocked (Fig. 2B) (*51*), which confirmed that loss of *dcr-1* reduces the number of embryonic cells undergoing cell death.

To investigate whether a general reduction in embryonic cell death may indirectly affect apoptotic DNA degradation, we performed the TUNEL assay on the *cps-1(sm24)* mutant, a CED-3 protease suppressor mutant that exhibits a cell-death defect similar to that of the *dcr-1(lf)* mutants (Fig. 2A) (*14*). Although *cps-1(sm24)* causes reduced embryonic cell death at most embryonic stages, as did the *dcr-1(lf)* mutations, it did not affect the number of TUNEL-stained cells in the *crn-2(tm1177)* embryos (Fig. 1D). This result suggests that, unlike *cps-1*, *dcr-1* facilitates cell death by promoting apoptotic DNA degradation.

We investigated whether reduction of embryonic cell death caused by *dcr-1(lf)* mutations might result in survival of cells that normally die and thus yield extra "undead" cells in the anterior pharynx of mutant animals (*14*, *49*). Both *dcr-1(ok247)* and *dcr-1(pk1351)* mutants had low numbers of extra cells in the anterior pharynx (table S1). When combined with other weak cell-death mutations, such as the partial loss-of-function mutation *(n2438)* in the gene encoding the CED-3 caspase, *dcr-1(lf)* mutations significantly increased the number of extra cells in the anterior pharynx (table S1). For example, an average of 1.3 extra cells were seen in *ced-3(n2438)* animals, whereas, on average, 3.1 extra cells were present in *dcr-1(lf); ced-3(n2438)* animals (table S1). Although *cps-6(sm116)* or *crn-2(tm1177)* individually also increased the number of extra cells in the *ced-3(n2438)* mutant background, neither *cps-6(sm116)* nor *crn-2(tm1177)* increased the number of extra cells in the *dcr-1(ok247); ced-3(n2438)* mutant (table S1), which indicated that *dcr-1*, *cps-6*, and *crn-2* may act in the same pathway to promote apoptosis and DNA degradation.

Because apoptotic DNA degradation occurs in response to caspase activation (*5*, *7*, *14*), we performed epistasis analysis to examine whether activation of *ced-3* leads to activation of *dcr-1*, using an integrated transgene (*smIs111*) expressing an activated form of CED-3 (acCED-3) under the control of the *egl-1* promoter (*49*, *52*). When *smIs111* was placed in the *ced-1(e1735); egl-1(n3082)* mutant background, in which almost all naturally occurring somatic cell deaths in *C. elegans* are blocked by a loss-of-function mutation (*n3082)* in the cell-death initiator *egl-1*, acCED-3 still induced ectopic cell death and an average of 16.5 and 11 persistent cell corpses in three-fold and four-fold late-stage embryos, respectively (Fig. 2C). The *dcr-1(ok247)* mutation significantly reduced the number of ectopic cell deaths induced by acCED-3 in *ced-1(e1735) smIs111; egl-1(n3082)* embryos, which indicated that *dcr-1* likely acts downstream of *ced-3* to promote apoptosis and DNA degradation.

DCR-1 cofactors in RNA processing do not affect apoptosis. In *C. elegans*, various cofactors interact with DCR-1 to regulate processing of dsRNA and to generate small RNAs, including miRNAs, siRNAs, and siRNAs derived from endogenous triggers (endo-siRNAs) (*21*, *26*, *53*). For example, ALG-1 and ALG-2 (Argonaute-like gene) are required for miRNA production; RDE-1, RDE-4, DRH-1, and DRH-2 are required for siRNA production; and ERI-1 and RRF-3 are required for endo-siRNA production. We thus examined whether these DCR-1 cofactors also functioned in regulating apoptosis and DNA degradation. Loss of DCR-1 cofactors did not affect the number of TUNEL-stained cells in the *cps-6(sm116)* mutant or *cps-6*(RNAi)–treated animals (table S2). Moreover, unlike *dcr-1(lf)* mutants, which have a reduced number of embryonic cell corpses, the numbers of embryonic cell corpses in animals deficient in DCR-1 cofactors were comparable to those seen in wild-type animals (fig. S1). These results indicate that defects in the generation of miRNAs, siRNAs, endo-siRNAs, or other small RNAs do not seem to affect apoptosis or apoptotic DNA degradation and that DCR-1 likely mediates apoptotic DNA degradation through a previously uncharacterized mechanism independent of its roles in RNA processing.

DCR-1 is a substrate of the CED-3 caspase. Given that *dcr-1* acts downstream of *ced-3* to promote apoptosis and DNA degradation, we tested whether DCR-1 itself might be a substrate of the CED-3 protease. We synthesized a glutathione *S*-transferase DCR-1 fusion (GST–DCR-1) and labeled it with [^{35}S]methionine in rabbit re-

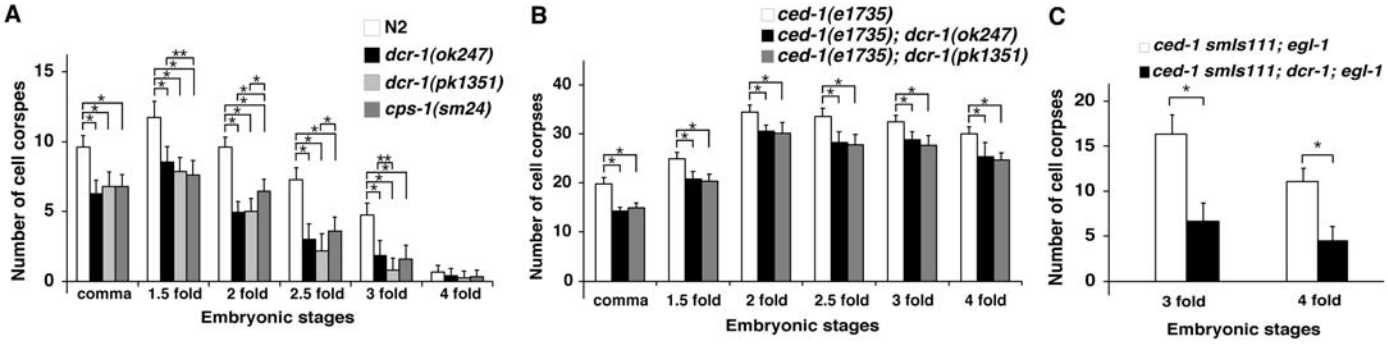

Fig. 2. Function of *dcr-1* downstream of *ced-3* to promote cell death. Embryonic cell corpses were counted in the following animals: (**A**) N2, *dcr-1(ok247)*, *dcr-1(pk1351)*, and *cps-1(sm24)* animals; (**B**) *ced-1(e1735)*, *ced-1(e1735); dcr-1(ok247)*, and *ced-1(e1735); dcr-1(pk1351)* animals; (**C**) *ced-1(e1735) smIs111; egl-1(n3082)* and *ced-1(e1735) smIs111; dcr-1(ok247); egl-1(n3082)* animals. Stages of embryos examined were comma, 1.5-fold, 2-fold, 2.5-fold, 3-fold, and 4-fold. The *y* axis represents average number of cell corpses scored, and error bars represent SD. For each embryonic stage, 15 embryos were counted. The significance of differences between different genetic backgrounds was determined by two-way ANOVA, followed by Bonferroni comparison. **P* < 0.001; ***P* < 0.05. All other points had *P* values > 0.05.

ticulocyte lysate and incubated it with purified CED-3 protease. [^{35}S]Met-labeled GST–DCR-1 was cleaved by CED-3, which yielded two primary cleavage products of about 193 and 43 kD (Fig. 3A, lanes 1 and 2). A DCR-1 deletion mutant, DCR-1(1045-1845), was also cleaved by CED-3 to yield the same 43-kD cleavage product (fig. S2A), which suggested that CED-3 cleavage occurs at the carboxyl terminus of DCR-1. To determine the CED-3 cleavage site in DCR-1, we expressed and purified a truncated DCR-1 protein with a six-histidine tag, DCR-1(1334-1791)-His$_6$, and incubated the purified protein with the CED-3 protease. The ~37-kD C-terminal DCR-1 cleavage product was subjected to N-terminal sequencing analysis (fig. S2B) (*49*). Residues 1473 to 1477 of DCR-1 (GIETI) (*39*) were found to be the N terminus of this DCR-1 cleavage product, which suggested that DCR-1 was cleaved by CED-3 between Asp^{1472} and Gly^{1473}. When Asp^{1472} of DCR-1 was replaced by Glu through site-directed mutagenesis, the resulting mutant protein GST–DCR-1(D1472E) was not cleaved by CED-3 (Fig. 3A, lanes 3 and 4), which confirmed that Asp^{1472} is the CED-3 cleavage site. Thus, DCR-1 is a substrate of CED-3 in vitro.

Cleavage of DCR-1 by CED-3 destroys the dsRNA dicing activity but activates a DNase activity. Full-length DCR-1 contains a helicase domain at its N terminus; a PAZ domain in the middle; and two RNase III–like domains (indicated as RNase IIIa and RNase IIIb, respectively) and a dsRNA binding domain at the C terminus (Fig. 3A). Cleavage of DCR-1 by CED-3 at Asp^{1472}, which is in the middle of the RNase IIIa domain, presumably would destroy the RNase IIIa domain but leave RNase IIIb unaffected. Consistent with the findings that both RNase III domains of Dicer are required for binding and cleaving dsRNA (*29*, *42*), CED-3 cleavage of GST–DCR-1 abolished the 22- to 23-nucleotide dicing activity of DCR-1 on dsRNA (Fig. 3A, left, lanes 5 to 8). However, the C-terminal cleavage product of DCR-1, which we named tDCR-1, still contains one intact RNase III domain (RNase IIIb) that may retain some endonuclease activity. Given that DCR-1 is also involved in mediating apoptotic DNA degradation, we examined whether DCR-1 or its CED-3 cleavage products might have a deoxyribonuclease activity. GST–DCR-1 and GST–DCR-1(D1472E) synthesized in rabbit reticulocyte lysate were affinity purified using glutathione Sepharose resins and incubated with pUC19 supercoiled plasmid DNA substrate in the presence or absence of the CED-3 protease (*49*). Purified CED-3 protease or GST–DCR-1 alone did not cleave or nick plasmid DNA (Fig. 3B, left, top, lanes 1 to 3). Incubation of CED-3 with GST–DCR-1 resulted in nicking of the plasmid DNA and the mobility shift of the plasmid DNA from the supercoiled form (SC) to the nicked open circle form (Fig. 3B, left, top, lane 4). This plasmid DNA nicking activity required the presence of Mg^{2+} and was not observed when GST–DCR-1(D1472E) was incubated with CED-3 (Fig. 3B,

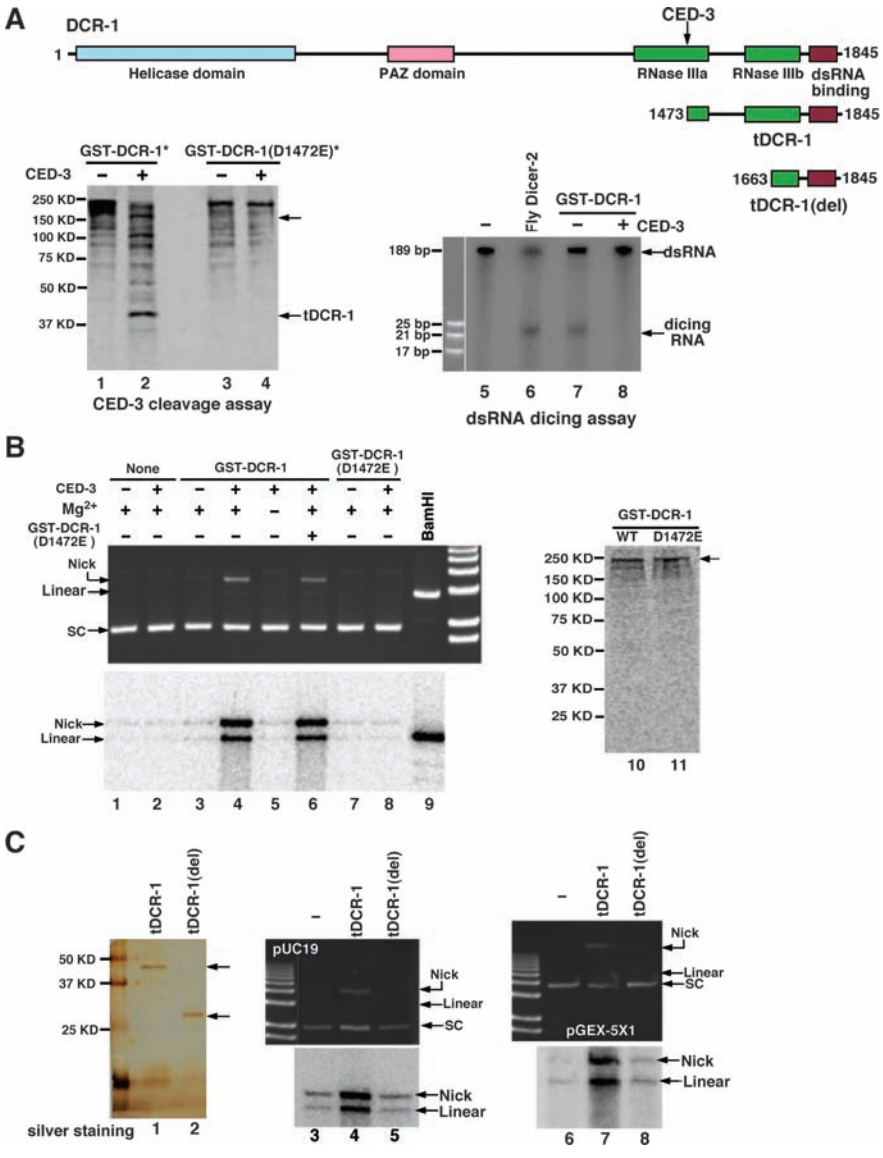

Fig. 3. Activation of a deoxyribonuclease activity after cleavage of DCR-1 by CED-3. (**A**) Cleavage of DCR-1 at Asp^{1472}. (Top) A schematic diagram of DCR-1, tDCR-1, tDCR-1(del), and various DCR-1 domains. The CED-3 cleavage site is indicated. (Bottom) Cleavage of DCR-1 by CED-3 at Asp^{1472} abolished the dsRNA dicing activity of DCR-1. (Lanes 1 to 4) GST–DCR-1 and GST–DCR-1(D1472E) were synthesized in rabbit reticulocyte lysate and labeled with [^{35}S]Met. They were then incubated with or without 5 ng of purified CED-3 for 1 hour and resolved by 12% SDS–polyacrylamide gel electrophoresis (PAGE). (Lanes 5 to 8) GST–DCR-1 was synthesized in rabbit reticulocyte lysate and purified by glutathione Sepharose resins. Purified GST–DCR-1 was first incubated with or without 5 ng of purified CED-3 for 2 hours before addition of [α-^{32}P]UTP–labeled dsRNA probes. Purified fly Dicer-2 protein was included as a positive control. Samples were resolved by 20% native polyacrylamide gel. Autoradiography image is shown. (**B**) Activation of DNase activity after cleavage of DCR-1 by CED-3. (Lanes 10 and 11) GST–DCR-1 and GST–DCR-1(D1472E) were synthesized and purified as in (A) in the presence of both Met and [^{35}S]Met (50:1). pUC19 plasmid DNA (200 ng) was incubated with purified GST–DCR-1 or GST–DCR-1(D1472E) or both (lane 6) in the presence or absence of 5 ng of purified CED-3 for 1 hour at 37°C (*49*). Twice the amount of GST–DCR-1(D1472E) was added in lane 6. One-half of the samples was resolved on 1% agarose gel and then stained with ethidium bromide before an ultraviolet image was taken (top). Two units of TdT, [α-^{32}P]dCTP, and $CoCl_2$ (250 μM) were added to the remaining reactions and incubated for another 2 hours at 37°C. The samples were resolved on 1% agarose gel, then fixed and dried for autoradiography (bottom). In lane 9, only one-fourth of the sample was loaded. A 1-kb Plus DNA ladder was used (Invitrogen). (**C**) DNase activity of tDCR-1. tDCR-1–Flag and tDCR-1(del)–Flag were expressed in *C. elegans*, purified on an anti-Flag affinity column, eluted by Flag peptides (*49*), and resolved on 15% SDS-PAGE, before being subjected to silver staining (lanes 1 and 2). The nuclease activity assay and TdT labeling were done as in (B) with two different plasmids (pUC19 and pGEX-5X1). The TdT labeling method is expected to more efficiently label a linear substrate versus a nicked substrate.

left, top, lanes 5, 7, 8), which indicated that CED-3 cleavage is required to activate this new Mg^{2+}-dependent DNase activity of DCR-1. Incubation of GST–DCR-1(D1472E) with GST–DCR-1 and CED-3 did not prevent the activation of this DNase activity by CED-3 (Fig. 3B, left, top, lane 6). Moreover, when the CED-3 cleavage site in DCR-1 was replaced by a site (ENLYFQG) (*39*) only recognized by the tobacco etch virus (TEV) protease (fig. S3A), the resulting DCR-1 mutant, GST–DCR-1(1472TEV), was not activated by CED-3 to generate a DNase activity (fig. S3B, lanes 1 to 4). By contrast, purified TEV protease cleaved GST–DCR-1(1472TEV) but not GST–DCR-1 to activate a similar DNase activity (fig. S3, A and B, lanes 5 to 10). Together, these results indicate that this CED-3–activated DNase activity is derived from cleavage of DCR-1 at Asp^{1472}

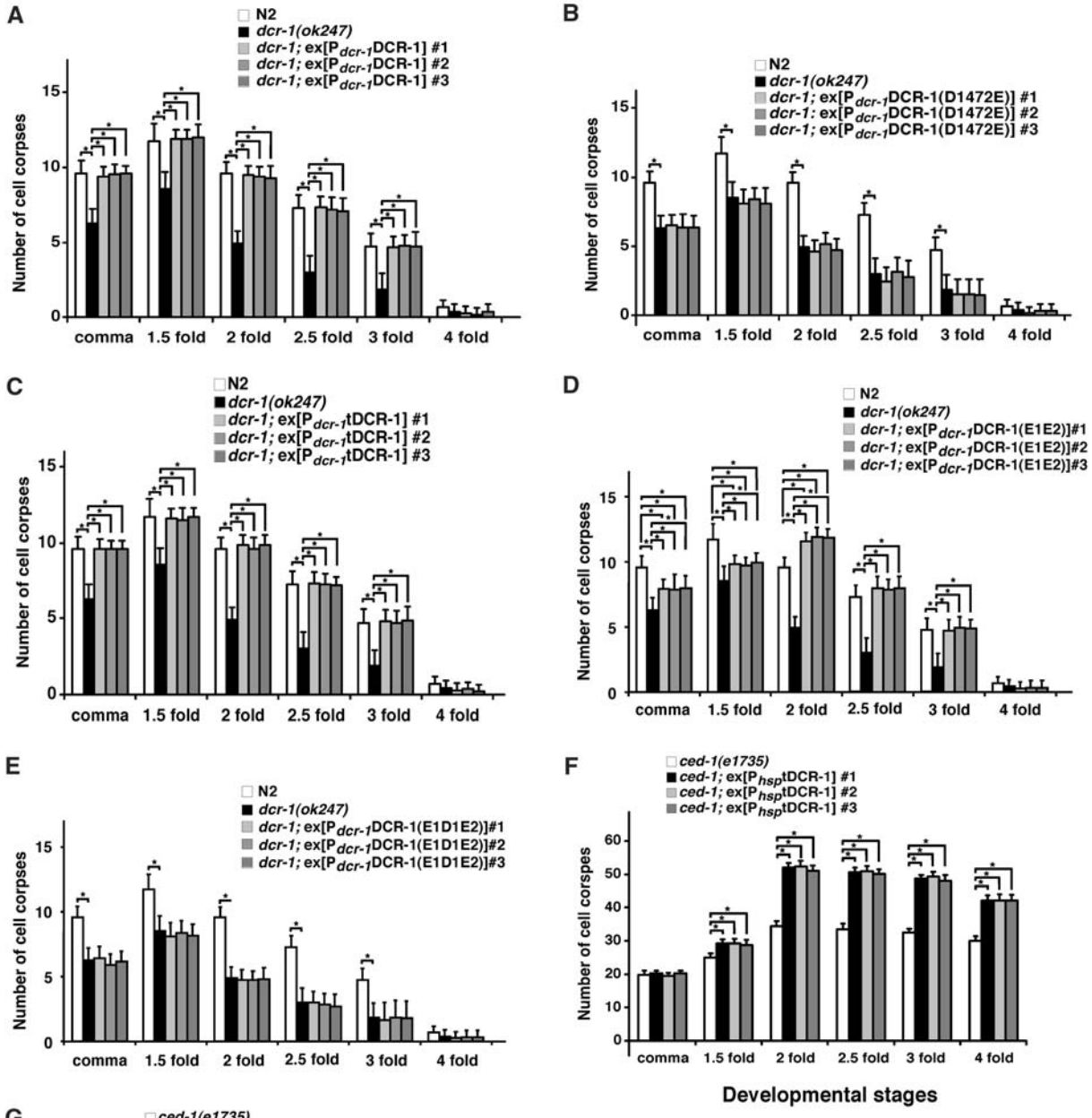

Fig. 4. Requirement of DCR-1 cleavage by CED-3 for its proapoptotic activity. Cell corpses were scored in the following animals: (**A**) N2, *dcr-1(ok247)*, *dcr-1(ok247); ex[$P_{dcr\text{-}1}$DCR-1]* arrays 1 to 3; (**B**) N2, *dcr-1(ok247)*, *dcr-1(ok247); ex[$P_{dcr\text{-}1}$DCR-1(D1472E)]* arrays 1 to 3; (**C**) N2, *dcr-1(ok247)*, *dcr-1(ok247); ex[$P_{dcr\text{-}1}$tDCR-1]* arrays 1 to 3; (**D**) N2, *dcr-1(ok247)*, *dcr-1(ok247); ex[$P_{dcr\text{-}1}$DCR-1(E1E2)]* arrays 1 to 3; (**E**) N2, *dcr-1(ok247)*, *dcr-1(ok247); ex[$P_{dcr\text{-}1}$DCR-1(E1D1E2)]* arrays 1 to 3; (**F**) *ced-1(e1735)*, *ced-1(e1735); ex[P_{hsp}tDCR-1]* arrays 1 to 3; and (**G**) *ced-1(e1735)*, *ced-1(e1735); ex[P_{hsp}tDCR-1(del)]* arrays 1 to 3. Stages of embryos examined were comma, 1.5-fold, 2-fold, 2.5-fold, 3-fold, and 4-fold. The *y* axis represents average number of cell corpses scored, and error bars represent SD. For each developmental stage, 15 embryos were counted. The significance of differences between different genetic backgrounds was determined by two-way ANOVA, followed by Bonferroni comparison. $*P < 0.001$; $**P < 0.05$. All other points had *P* values > 0.05.

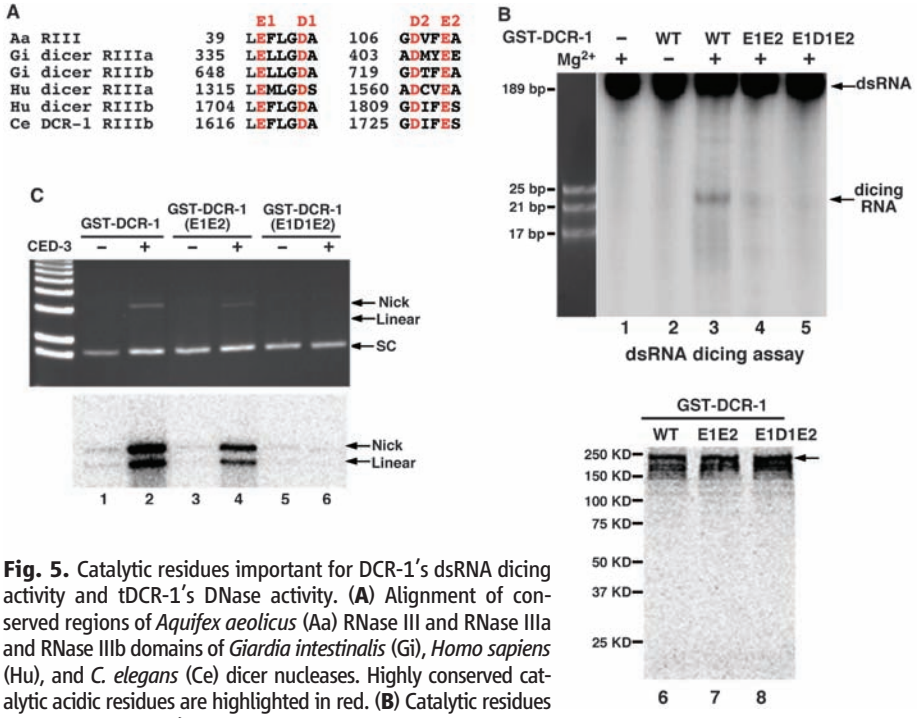

Fig. 5. Catalytic residues important for DCR-1's dsRNA dicing activity and tDCR-1's DNase activity. (**A**) Alignment of conserved regions of *Aquifex aeolicus* (Aa) RNase III and RNase IIIa and RNase IIIb domains of *Giardia intestinalis* (Gi), *Homo sapiens* (Hu), and *C. elegans* (Ce) dicer nucleases. Highly conserved catalytic acidic residues are highlighted in red. (**B**) Catalytic residues important for DCR-1's dsRNA dicing activity. (Top) The dsRNA dicing assay was done as in Fig. 3A. Wild-type (WT) and mutant GST—DCR-1 proteins (E1E2 and E1D1E2), in which the indicated acidic residues were replaced by Ala, were synthesized and purified as in Fig. 3B. (Bottom) Purified GST—DCR-1 proteins. (**C**) Catalytic residues important for tDCR-1's DNase activity. The DNase activity assay on the pUC19 plasmid and TdT labeling were done as in Fig. 3B.

rather than from a protein copurified with DCR-1 and activated by CED-3 cleavage.

Because the RNase III enzyme is known to generate 3′ OH ends (*30*, *40*) and DCR-1 is implicated in generating 3′ OH DNA breaks in *C. elegans* apoptotic cells that are labeled by TUNEL (Fig. 1), we tested whether CED-3–activated DCR-1 produced 3′ OH ends in vitro that could be labeled by [α-^{32}P]deoxycytidine triphosphate (dCTP) catalyzed by TdT. Bam HI, a restriction endonuclease, completely linearized plasmid DNA and generated 3′ OH DNA ends that were strongly labeled by TdT (Fig. 3B, left, bottom, lane 9). GST–DCR-1 but not GST–DCR-1(D1472E), when treated with CED-3, generated both nicked and linearized plasmid DNAs that were labeled by TdT in a Mg^{2+}-dependent manner (Fig. 3B, left, bottom, lanes 3 to 8). This result indicates that cleavage of DCR-1 by CED-3 activates a deoxyribonuclease activity that can nick DNA and create 3′ OH ends.

tDCR-1 has the DNase activity. We further investigated whether tDCR-1, a CED-3 cleavage product that retains a complete RNase IIIb domain and a dsRNA-binding domain, is responsible for the newly generated DNase activity. tDCR-1 tagged with a Flag epitope was expressed in *C. elegans* under the control of heat-shock promoters. A mutant tDCR-1, in which one-half of the RNase IIIb domain is deleted [tDCR-1(del)], was similarly expressed in *C. elegans*. After heat-shock induction, tDCR-1–Flag and tDCR-1(del)–Flag were purified from worm lysate on an anti-Flag affinity column (Fig. 3C, lanes 1and 2) (*49*) and tested for the DNase activity. tDCR-1 nicked supercoiled plasmid DNA and caused a shift of some of the DNA to the nicked open circle form, whereas tDCR-1(del)–Flag failed to do so (Fig. 3C, top, lanes 3 to 5). TdT labeling indicated that tDCR-1 generated both nicked and linearized plasmid DNAs with 3′ OH ends (Fig. 3C, bottom, lane 4), whereas tDCR-1(del) did not nick or linearize plasmid DNA. We observed similar results with two other plasmids with different sizes (Fig. 3C, lanes 6 to 8 and fig. S3C), which indicated that the nicking activity of tDCR-1 may be relatively unspecific as to sequence. Thus, tDCR-1 functions as a DNase to nick DNA and to generate 3′ OH ends.

Cleavage of DCR-1 by CED-3 is important for its proapoptotic activity. We tested whether cleavage of DCR-1 by CED-3 is required for promoting cell death in *C. elegans*. Expression of DCR-1 under the control of the endogenous *dcr-1* promoter ($P_{dcr\text{-}1}$DCR-1) fully rescued the reduced-embryonic-cell-corpse phenotype of *dcr-1(ok247)* animals (Fig. 4A). This construct also rescued the abnormal vulva phenotype (bursting vulva and protruding vulva) of *dcr-1(ok247)* animals (table S3), which is due to a defect in biogenesis of miRNAs (*21*). We were unable to examine rescue of the RNAi defect of *dcr-1(ok247)* animals, because *dcr-1(ok247)* homozygous animals derived from *dcr-1(ok247)*/+ heterozygous mothers show no RNAi defect owing to maternal rescue of *dcr-1* (*21*). $P_{dcr\text{-}1}$DCR-1(D1472E), which drives the expression of the CED-3–resistant DCR-1 mutant, rescued the vulva defects of *dcr-1(ok247)* animals, but failed to rescue the reduced-embryonic-cell-corpse phenotype of *dcr-1(ok247)* animals (table S3 and Fig. 4B). These findings indicate that cleavage of DCR-1 by CED-3 is critical for promoting cell death but is not needed for biogenesis of miRNAs. However, expression of tDCR-1 under the control of the *dcr-1* promoter ($P_{dcr\text{-}1}$tDCR-1) fully rescued the cell-death defect of *dcr-1(ok247)* animals but did not rescue their vulva defects (Fig. 4C and table S3), which confirmed that tDCR-1 is sufficient to mediate DCR-1's proapoptotic function.

We generated three integrated transgenes, *smIs182*, *smIs196*, and *smIs201*, which carry $P_{dcr\text{-}1}$DCR-1, $P_{dcr\text{-}1}$DCR-1(D1742E), and $P_{dcr\text{-}1}$tDCR-1, respectively. These transgenes were crossed into the *cps-6(sm116); dcr-1(ok247)* mutant, and we assessed their ability to rescue the DNA degradation defect of the *dcr-1(ok247)* mutant. Both *smIs182* ($P_{dcr\text{-}1}$DCR-1) and *smIs201* ($P_{dcr\text{-}1}$tDCR-1) restored the number of TUNEL-stained cells in *cps-6(sm116); dcr-1(ok247)* embryos to the level seen in *cps-6(sm116)* embryos alone (Fig. 1E), which suggested that both transgenes rescue the DNA degradation defect of the *dcr-1(ok247)* mutant. In contrast, *cps-6(sm116); dcr-1(ok247)*; *smIs196* embryos had few TUNEL-stained cells (Fig. 1E), which indicated that the $P_{dcr\text{-}1}$DCR-1(D1742E) transgene was unable to rescue the DNA degradation defect of the *dcr-1(ok247)* mutant. These results further indicate that tDCR-1 is sufficient to replace DCR-1 in promoting DNA degradation and apoptosis, whereas the CED-3–resistant DCR-1 mutant is not.

We also induced global overexpression of tDCR-1 under the control of the heat-shock promoters (P_{hsp}tDCR-1) and examined whether tDCR-1 could induce ectopic apoptosis. When expressed in the *ced-1(e1735)* mutant that is defective in engulfment of apoptotic cells and thus allows easy detection of increased apoptosis, tDCR-1 caused an increase of about 45 to 50% in the number of apoptotic cells (Fig. 4F), whereas the DNase-defective tDCR-1(del) mutant had no such activity (Fig. 4G). In the strong *ced-3(n2433)* mutant that is deficient in cell death, tDCR-1 overexpression failed to induce any apoptosis (table S4), possibly because tDCR-1 needs to cooperate with other CED-3–activated cell-death pathways to induce apoptosis. Yet overexpression of tDCR-1 but not tDCR-1(del) still created a significant number of TUNEL-stained cells (Fig.1G), which showed that tDCR-1 can initiate 3′ OH nicks in chromosomal DNA, independently of CED-3. Together, these results indicate that cleavage of DCR-1 by CED-3 during apoptosis is critical for its role in promoting apoptosis and produces a cleavage product, tDCR-1, that initiates apoptotic DNA degradation through its DNase activity.

Conserved acidic residues are important for both DCR-1 cleavage of RNA and tDCR-1 cleavage of DNA. Because DCR-1 is a dsRNA-processing enzyme and the yeast RNA III,

Rnt1p, can cleave the DNA strand of DNA-RNA hybrids in vitro (*54*), tDCR-1 may cleave DNA through the same catalytic mechanism used for dsRNA cleavage. We thus examined whether catalytic residues that are critical for Dicer's ribonuclease activity are also important for tDCR-1's DNase activity (*29*, *42*). Structural analysis of *Giardia* Dicer reveals four highly conserved acidic residues that are involved in binding and positioning of the two catalytic divalent metal cations in each RNase III domain (Fig. 5A; they are named E1, D1, D2, and E2 for simplicity) (*42*). The D1 and E2 residues in both RNase III domains have been shown to be important for the dicing activity of human dicer (*29*). We generated two DCR-1 mutants with altered acidic residues in the RNase IIIb domain, the E1E2 double mutant (E1617A, E1729A) and the E1D1E2 triple mutant (E1617A, D1621A, E1729A). We then assayed their dsRNA dicing activity and CED-3–activated DNase activity. The DCR-1(E1E2) mutant showed significantly reduced dsRNA dicing activity, which was dependent on the presence of Mg^{2+} (Fig. 5B, lanes 1 to 4). The CED-3–activated DNase activity of DCR-1(E1E2) was also impaired (Fig. 5C, lanes 1 to 4). In comparison, no detectable dsRNA dicing activity or CED-3–activated DNase activity was observed with the DCR-1(E1D1E2) triple mutant (Fig. 5B, lane 5, and Fig. 5C, lanes 5 to 6). These results and the observations that the dsRNA dicing activity and the CED-3–activated DNase activity of DCR-1 were both dependent on Mg^{2+} indicate that the catalytic mechanism of DNA cleavage by tDCR-1 is likely similar to that for dsRNA cleavage by DCR-1. They also provide further evidence that the CED-3–activated DNase activity comes from Dicer.

We also tested whether these catalytic residues are important for DCR-1's functions in vivo. Consistent with its reduced RNase and DNase activities in vitro, DCR-1(E1E2) expressed under the control of the *dcr*-1 promoter [$P_{dcr\text{-}1}$DCR-1(E1E2)] partially rescued the vulva defects, the reduced-embryonic-cell-corpse defect, and the DNA degradation defect of *dcr-1(ok247)* animals (table S3, and Figs. 1F and 4D). However, expression of the DCR-1(E1D1E2) mutant [$P_{dcr\text{-}1}$DCR-1(E1D1E2)], which had no detectable RNase or DNase activity in vitro (Fig. 5, B and C), failed to rescue all three defects of *dcr-1(ok247)* animals that we assayed (table S3, Fig. 1F, and Fig. 4E). Thus, the in vitro dsRNA dicing activity and the CED-3–activated DNase activity of two DCR-1 mutants correlate with their abilities to promote small RNA processing and apoptosis in *C. elegans*.

Discussion. The Dicer ribonuclease plays a critical role in processing dsRNA substrates into short dsRNA species, such as siRNAs and miRNAs with diverse regulatory functions (*30*, *40*, *41*). Our findings that *C. elegans* DCR-1 is involved in generating TUNEL-reactive DNA breaks in apoptotic cells that are later resolved by downstream apoptotic nucleases, such as CPS-6 and NUC-1, and that DCR-1 promotes, and even is required for, apoptosis in sensitized genetic backgrounds reveal an unexpected role of DCR-1 in apoptosis and in initiating apoptotic DNA degradation. The observations that inactivation of crucial DCR-1 cofactors in generating siRNAs, miRNAs, endo-siRNAs, and other small RNAs did not affect either apoptotic DNA degradation or apoptosis indicate that DCR-1 likely promotes apoptosis through a distinct mechanism that is not related to dsRNA processing and gene silencing.

Dicer is a member of the RNase III family that recognizes and cleaves dsRNA substrates to various lengths and is not known to contain a deoxyribonuclease activity (*40*, *41*). All RNase III family enzymes contain at least one characteristic RNase III domain and most also have a dsRNA-binding domain (dsRBD). Some, like Dicer, contain two RNase III domains and several additional domains, including the PAZ domain and the DExH helicase domain. Biochemical and structural analyses of the Dicer enzymes indicate that two RNase III domains form an intramolecular dimer, which constitutes a single processing center, with each domain contributing to the hydrolysis of one RNA strand of the duplex substrate through several highly conserved acidic residues that bind and position two catalytic Mg^{2+} cations (*29*, *42*). Interestingly, CED-3 cleaves *C. elegans* DCR-1 in the middle of its first RNase III domain, yielding a C-terminal cleavage product (tDCR-1) with only one complete RNase III domain, and presumably, a disabled dsRNA processing center. Indeed, cleavage of DCR-1 by CED-3 abolishes the dsRNA dicing activity of DCR-1. However, cleavage of DCR-1 by CED-3 appears to also activate a deoxyribonuclease activity that can nick and linearize DNA to generate 3′ OH DNA ends through the same highly conserved catalytic residues and Mg^{2+} cations, and this DNase activity is not observed in full-length DCR-1. The observations that tDCR-1 similarly nicked and linearized DNA in vitro and fully rescued the cell-death defects of the *dcr-1(lf)* mutant when expressed under the control of the *dcr-1* promoter and the findings that expression of DCR-1(D1472E), the CED-3–resistant mutant, fully rescued the developmental defects of the *dcr-1(lf)* mutant but failed to rescue the cell-death defects of the *dcr-1(lf)* mutant indicate that cleavage of the DCR-1 ribonuclease by CED-3 activates a DNase activity that is necessary and sufficient to promote DNA degradation and apoptosis and that the proapoptotic function of DCR-1 is separable from DCR-1's developmental functions. The proteolytic mechanism we discovered, through which a ribonuclease is disabled and converted into a DNase, may have more general implications on regulation of RNases and DNases, RNA and DNA binding proteins, and their associated cellular functions.

In mammals, the apoptotic nuclease DFF40 is kept in check in normal cells by its cognate inhibitor DFF45 (*5*–*8*). During apoptosis, executor caspases, such as caspase-3 and caspase-7, are activated to cleave a plethora of caspase targets, which lead to rapid cell disassembly. One of these targets is DFF45, which is cleaved and inactivated by caspases to unleash DFF40 and to initiate the chromosome fragmentation process. It is intriguing that no DFF40 or DFF45 homologs are found in *C. elegans*, in which other key cell-death components are highly conserved, including apoptotic nucleases endoG and DNase II (*4*). We propose that tDCR-1 is a functional analog of DFF40 and that a conserved, caspase-mediated mechanism activates the apoptotic DNA degradation process in both *C. elegans* and mammals.

References and Notes

1. A. H. Wyllie, *Nature* **284**, 555 (1980).
2. P. Widlak, W. T. Garrard, *J. Cell. Biochem.* **94**, 1078 (2005).
3. K. Samejima, W. C. Earnshaw, *Nat. Rev. Mol. Cell Biol.* **6**, 677 (2005).
4. J. Z. Parrish, D. Xue, *Chromosoma* **115**, 89 (2006).
5. X. Liu, H. Zou, C. Slaughter, X. Wang, *Cell* **89**, 175 (1997).
6. X. Liu *et al*., *Proc. Natl. Acad. Sci. U.S.A.* **95**, 8461 (1998).
7. M. Enari *et al*., *Nature* **391**, 43 (1998).
8. H. Sakahira, M. Enari, S. Nagata, *Nature* **391**, 96 (1998).
9. P. Widlak, P. Li, X. Wang, W. T. Garrard, *J. Biol. Chem.* **275**, 8226 (2000).
10. F. Durrieu *et al*., *Curr. Biol.* **10**, 923 (2000).
11. J. Zhang *et al*., *Proc. Natl. Acad. Sci. U.S.A.* **95**, 12480 (1998).
12. K. Kawane *et al*., *Nat. Immunol.* **4**, 138 (2003).
13. L. Y. Li, X. Luo, X. Wang, *Nature* **412**, 95 (2001).
14. J. Parrish *et al*., *Nature* **412**, 90 (2001).
15. S. Büttner *et al*., *Mol. Cell* **25**, 233 (2007).
16. J. Z. Parrish, D. Xue, *Mol. Cell* **11**, 987 (2003).
17. J. Z. Parrish, C. Yang, B. Shen, D. Xue, *EMBO J.* **22**, 3451 (2003).
18. Y. C. Wu, G. M. Stanfield, H. R. Horvitz, *Genes Dev.* **14**, 536 (2000).
19. S. M. Hammond, E. Bernstein, D. Beach, G. J. Hannon, *Nature* **404**, 293 (2000).
20. E. Bernstein, A. A. Caudy, S. M. Hammond, G. J. Hannon, *Nature* **409**, 363 (2001).
21. A. Grishok *et al*., *Cell* **106**, 23 (2001).
22. G. Hutvágner *et al*., *Science* **293**, 834 (2001).
23. S. W. Knight, B. L. Bass, *Science* **293**, 2269 (2001).
24. J. W. Pham, J. L. Pellino, Y. S. Lee, R. W. Carthew, E. J. Sontheimer, *Cell* **117**, 83 (2004).
25. Y. S. Lee *et al*., *Cell* **117**, 69 (2004).
26. T. F. Duchaine *et al*., *Cell* **124**, 343 (2006).
27. S. M. Elbashir, W. Lendeckel, T. Tuschl, *Genes Dev.* **15**, 188 (2001).
28. H. Zhang, F. A. Kolb, V. Brondani, E. Billy, W. Filipowicz, *EMBO J.* **21**, 5875 (2002).
29. H. Zhang, F. A. Kolb, L. Jaskiewicz, E. Westhof, W. Filipowicz, *Cell* **118**, 57 (2004).
30. M. A. Carmell, G. J. Hannon, *Nat. Struct. Mol. Biol.* **11**, 214 (2004).
31. Q. Liu *et al*., *Science* **301**, 1921 (2003).
32. J. Liu *et al*., *Science* **305**, 1437 (2004).
33. F. V. Rivas *et al*., *Nat. Struct. Mol. Biol.* **12**, 340 (2005).
34. R. W. Carthew, E. J. Sontheimer, *Cell* **136**, 642 (2009).
35. H. Tabara, E. Yigit, H. Siomi, C. C. Mello, *Cell* **109**, 861 (2002).
36. H. Tabara *et al*., *Cell* **99**, 123 (1999).
37. F. Simmer *et al*., *Curr. Biol.* **12**, 1317 (2002).
38. S. Kennedy, D. Wang, G. Ruvkun, *Nature* **427**, 645 (2004).
39. Single-letter abbreviations for the amino acid residues are as follows: A, Ala; C, Cys; D, Asp; E, Glu; F, Phe; G, Gly; H, His; I, Ile; K, Lys; L, Leu; M, Met; N, Asn; P, Pro; Q,

Gln; R, Arg; S, Ser; T, Thr; V, Val; W, Trp; Y, Tyr; and x, any amino acid
40. I. J. MacRae, J. A. Doudna, *Curr. Opin. Struct. Biol.* **17**, 138 (2007).
41. L. Jaskiewicz, W. Filipowicz, *Curr. Top. Microbiol. Immunol.* **320**, 77 (2008).
42. I. J. MacRae *et al.*, *Science* **311**, 195 (2006).
43. K. Mochizuki, N. A. Fine, T. Fujisawa, M. A. Gorovsky, *Cell* **110**, 689 (2002).
44. T. A. Volpe *et al.*, *Science* **297**, 1833 (2002).
45. E. Bernstein *et al.*, *Nat. Genet.* **35**, 215 (2003).
46. D. Baulcombe, *Nature* **431**, 356 (2004).
47. S. D. Hatfield *et al.*, *Nature* **435**, 974 (2005).
48. K. Förstemann *et al.*, *PLoS Biol.* **3**, e236 (2005).
49. Materials and methods are available as supporting material on *Science* Online.
50. G. M. Stanfield, H. R. Horvitz, *Mol. Cell* **5**, 423 (2000).
51. R. E. Ellis, D. M. Jacobson, H. R. Horvitz, *Genetics* **129**, 79 (1991).
52. D. Kokel, Y. Li, J. Qin, D. Xue, *Nat. Chem. Biol.* **2**, 338 (2006).
53. D. M. Pavelec, J. Lachowiec, T. F. Duchaine, H. E. Smith, S. Kennedy, *Genetics* **183**, 1283 (2009).
54. B. Lamontagne, R. N. Hannoush, M. J. Damha, S. Abou Elela, *J. Mol. Biol.* **338**, 401 (2004).
55. We thank T. Blumenthal, N. Pace, M. Yarus, L. He, X. D. Liu, and S. Marquez for comments; Y. Kohara for *dcr-1* cDNA; Q. H. Liu for purified fly Dicer-2 protein; K. Morita for the *alg-1* RNAi construct; and members of the Xue lab for helpful discussions. This work was supported by a Burroughs Wellcome Fund Award (D.X.), a grant from Ministry of Education, Culture, Sports, Science and Technology (MEXT) of Japan (S.M.), and NIH grants R01 GM59083 and R01 GM79097 (D.X.).

Supporting Online Material

www.sciencemag.org/cgi/content/full/science.1182374/DC1
Materials and Methods
Figs. S1 to S3
Tables S1 to S4
References

23 September 2009; accepted 1 March 2010
Published online 11 March 2010;
10.1126/science.1182374
Include this information when citing this paper.

REPORTS

Detection of a Large-Scale Structure of Intracluster Globular Clusters in the Virgo Cluster

Myung Gyoon Lee,[1]* Hong Soo Park,[1] Ho Seong Hwang[1,2]

Globular clusters are usually found in galaxies, and they are excellent tracers of dark matter. Long ago it was suggested that intracluster globular clusters (IGCs) may exist that are bound to a galaxy cluster rather than to any single galaxy. Here we present a map showing the large-scale distribution of globular clusters over the entire Virgo cluster. It shows that IGCs are found out to 5 million light years from the Virgo center and that they are concentrated in several substructures that are much larger than galaxies. These objects might have been mostly stripped off from low-mass dwarf galaxies.

Almost six decades ago, it was suggested that stars and interstellar medium may exist between galaxies that are in clusters of galaxies (*1*, *2*). To date, there is accumulating evidence for the existence of diffuse optical stellar light, planetary nebulae, resolved red giant stars, and diffuse hot x-ray–emitting gas between galaxies in nearby galaxy clusters (*3*–*7*). Some of these objects are not bound to any single galaxy but are gravitationally controlled by the potential of the galaxy cluster itself. These are called intracluster objects.

It was then suggested that globular clusters should be stripped off from galaxies in a galaxy cluster and that there should be a cluster-wide population of intracluster globular clusters (IGCs) in galaxy clusters (*8*–*10*). However, so far there has been no indication of IGCs in the Coma cluster, and only a small number of IGCs were found in similar studies of other galaxy clusters because of the studies' relatively shallow photometric limits or small area coverage (*11*–*14*). It is not yet known whether this cluster-wide population of IGCs exists in any galaxy cluster or not.

The Virgo cluster is the best target in which to search for a cluster-wide population of IGCs, because it is the nearest massive galaxy cluster. However, because of its largest angular extent (over 10° in the sky) (*15*) and the faintness of its globular clusters, it has been difficult to find and study IGCs over the entire Virgo cluster.

We present the results of a search for globular clusters over the entire Virgo cluster using data from the Sloan Digital Sky Survey (SDSS) (*16*, *17*). The SDSS data are deep enough to study the bright globular clusters in Virgo, and its survey area is wide enough to cover the entire Virgo cluster.

The Virgo cluster is located at a distance of 54 million light years (16.5 mpc); 1° in the sky corresponds to 940,000 light years (288 kpc) at this distance. The globular clusters at the distance of Virgo appear as point sources in the SDSS images; thus, they cannot be distinguished from faint foreground stars in our Galaxy in the images. To overcome this problem and create a map of the globular clusters in Virgo, we used the photometry of the point sources in the SDSS Sixth Data Release (*18*).

We selected bright globular cluster candidates in a circular field with a radius of 9°, including the Virgo cluster, using the criteria for color and magnitude (with reddening corrected): $0.6 < (g-i)_0 < 1.3$ and $19.5 < i_0 < 21.7$ mag (where g and i are

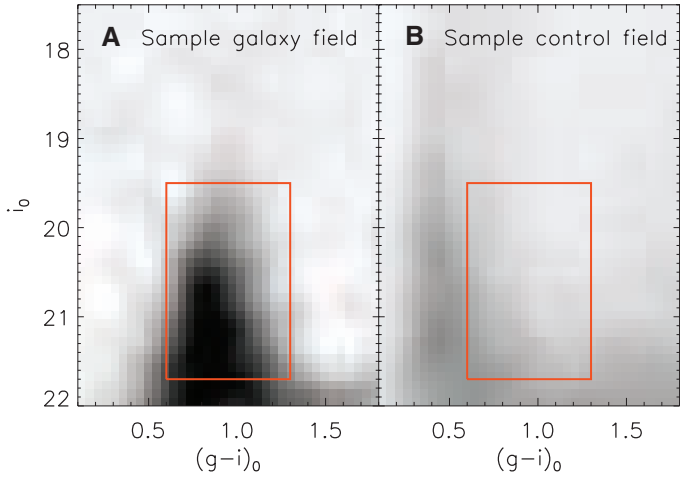

Fig. 1. $i_0 - (g-i)_0$ color-magnitude diagrams for the point sources in Virgo. (**A**) A sample galaxy field composed of 10 circular fields (radius 20 arc min) centered on the brightest galaxies. The contribution of the foreground stars was subtracted. Most of the sources are globular clusters. (**B**) A sample control field located at 6° to 9° from the Virgo center, covering the same area as (A). Most of the sources are foreground stars belonging to our Galaxy. Darker colors represent the higher number density. The box represents the region used for selecting the bright globular cluster candidates in Virgo in this study.

[1]Astronomy Program, Department of Physics and Astronomy, Seoul National University, Seoul 151-742, Korea. [2]CEA Saclay/Service d'Astrophysique, F-91191 Gif-sur-Yvette, France.

*To whom correspondence should be addressed. E-mail: mglee@astro.snu.ac.kr

Supporting Online Material for

Caspase-Dependent Conversion of Dicer Ribonuclease into a Death-Promoting Deoxyribonuclease

Akihisa Nakagawa, Yong Shi, Eriko Kage-Nakadai, Shohei Mitani, Ding Xue*

*To whom correspondence should be addressed. E-mail: ding.xue@colorado.edu

Published 11 March 2010 on *Science* Express
DOI: 10.1126/science.1182374

This PDF file includes

Materials and Methods

Strains and culture conditions

C. elegans strains were maintained using standard procedures (*S1*). The following alleles were used in the genetic analyses: LGI, *ced-1(e1735), dpy-5(e61)*, *cps-6(sm116)*, *cps-1(sm24), drh-3(tm1217), smIs111, hT2[bli-4(e937) let-?(q782) qIs48]* (I, III); LGII, *alg-2(ok304)*, *pir-1(tm1496)*, *rrf-3(pk1426)*; LGIII, *dcr-1(ok247, pk1351)*, *rde-4(ne301)*; LGIV, *ced-3(n2433, n2438)*, *drh-1(tm1329)*, *drh-2(ok951);* LGV, *egl-1(n3082), eri-1(mg366)*, *rde-1(ne219)*, *crn-2(tm1177)*; LGX, *nuc-1(e1392)*, *alg-1(gk214)*. *smIs182*, *smIs196* and *smIs201* were integrated transgenes generated by gamma irradiation of animals carrying extrachromosomal arrays containing $P_{dcr\text{-}1}$DCR-1, $P_{dcr\text{-}1}$DCR-1(D1742E), and $P_{dcr\text{-}1}$tDCR-1, respectively. They were backcrossed four times with N2 animals before being used for genetic analyses.

Quantification of cell corpses and extra cells

The number of cell corpses in living embryos and the number of extra cells in the anterior pharynx of L4 larvae were scored using Nomarski optics as described previously (*S2*).

Transgenic animals

Transgenic animals were generated as described previously (*S3*). $P_{dcr\text{-}1}$DCR-1, $P_{dcr\text{-}1}$tDCR-1, $P_{dcr\text{-}1}$DCR-1(D1472E), $P_{dcr\text{-}1}$DCR-1(E1E2), or $P_{dcr\text{-}1}$DCR-1(E1D1E2) was injected into either N2 or *dcr-1(ok247)/hT2* animals at 1 μg/ml along with the pTG96 plasmid (at 20 μg/ml) as a co-injection marker. The pTG96 plasmid contains a *sur-5::gfp* translational fusion that is expressed in all somatic cells in most developmental stages

(*S4*). P_{hsp}tDCR-1-FLAG or P_{hsp}tDCR-1(del)-FLAG was injected into N2 at 20 μg/ml along with the pTG96 plasmid (at 40 μg/ml). The transgenic arrays were then crossed into the *dcr-1(ok247)/hT2, ced-3(n2433)* or *ced-1(e1735)* background.

Heat shock experiments

100 gravid transgenic adults were placed on plates at 20°C for 3 hours to let them lay eggs. The plates were then heat-shocked at 33°C for 45 minutes and returned to 20°C for 75 min before removing all adults. After two more hours at 20°C, the transgenic embryos were scored for the number of cell corpses.

RNAi experiments

RNAi experiments were carried out using a bacteria feeding protocol described previously (*S5*).

TUNEL assays and antibody staining

The TUNEL assays were carried out as described previously (*S2*), using *in situ* cell-death detection kit (Roche). For TUNEL/antibody double staining, mix-stage animals were harvested with M9 and bleached with 12% NaOCl and 1.5 M NaOH to obtain embryos, which were then centrifuged at 500 x g to remove bacteria and debris of larvae and adults. Embryos were washed several times with ddH_2O, fixed with a fixation solution [40% MeOH, 3% Paraformaldehyde, 0.2% spermine, 100 mM KCl, 30 mM NaCl, 12.5 mM HEPES (pH 7.0), and 2 mM EGTA], and frozen in liquid nitrogen for 45 minutes. Following that, embryos were thawed at 37°C, first washed with 100 mM Tris (pH7.0)

and 1% Triton X-100, and subsequently washed with PBST (PBS and 0.5% Triton X-100). Embryos were then stained with anti-GFP monoclonal antibody (Zymed) at 0.15 mg/ml in PBST for 1 hour. After embryos were washed 3 times with PBST, they were stained with TUNEL and rhodamine-conjugated anti-mouse IgG antibody (Jackson ImmunoResearch) at 1/100 dilution in PBST for 1 hour. Embryos were washed twice with PBST and mounted on slides with mounting medium containing DAPI (VECTOR).

Molecular biology

A partial *dcr-1* cDNA clone, yk24e10, was kindly provided by Dr. Yuji Kohara. The rest of *dcr-1* cDNA was amplified using reverse transcription polymerase chain reaction (RT-PCR) and then fused with the yk24e10 clone to generate the full-length *dcr-1* cDNA clone. Standard molecular cloning methods were employed to make pET-41b-DCR-1, pET-30b-DCR-1(1045-1845), and pET-30b-DCR-1(1334-1791) clones. Briefly, full-length *dcr-1* cDNA was subcloned into the pET-41b vector via its Spe I and Kpn I sites to generate the pET-41b-DCR-1 expression vector. A BamH I-Xho I *dcr-1* cDNA fragment encoding amino acids 1045 to 1845 (resulting from Xho I partial digestion) and a Hpa I-Xho I *dcr-1* cDNA fragment encoding amino acids 1334 to 1791 were excised from the full-length *dcr-1* cDNA clone and inserted into the pET-30b vector via its BamHI/Xho I and EcoR V/Xho I sites, respectively, to generate pET-30b-DCR-1(1045-1845) and pET-30b-DCR-1(1334-1791). To construct P_{dcr-1}DCR-1, a 13045 bp Avr II-Eag I *dcr-1* genomic fragment that contains 4654 bp of the *dcr-1* promoter sequence, 8165 bp of the *dcr-1* coding sequence, and 226 bp of the *dcr-1* 3' untranslated region (UTR) was excised from the fosmid clone wrm066bH04 and subcloned into the

pBluescript SKII (+) vector through its Spe I and Eag I sites. To construct P_{dcr-1}tDCR-1, P_{dcr-1}DCR-1(D1472E), P_{dcr-1}DCR-1(E1E2), and P_{dcr-1}DCR-1(E1D1E2), P_{dcr-1}DCR-1 was used as a DNA template to remove the *dcr-1* genomic region encoding amino acids 2 to 1472 or to make the indicated amino acid substitutions using PCR-based Quick Change mutagenesis kit (Stratagene). These expression constructs therefore contain the same translation signals. All clones were confirmed by DNA sequencing. To construct P_{hsp}tDCR-1-FLAG and P_{hsp}tDCR-1(del)-FLAG, a cDNA fragment encoding DCR-1 amino acids 1473 to1845 or amino acids 1663 to 1845 was amplified and tagged with a FLAG epitope by PCR and subcloned into *C. elegans* heat shock vectors, pPD49.78 and pPD49.83. These expression constructs have the same translation signals derived from the heat-shock promoters. pET-41b-DCR-1(D1472E), pET-41b-DCR-1(E1E2), pET-41b-DCR-1(E1D1E2), and pET-41b-DCR-1(1472TEV) were similarly made through Quick Change mutagenesis. In pET-41b-DCR-1(1472TEV), Asp 1472 was replaced with ENLYFQ, a TEV cleavage site.

Protein expression and purification

DCR-1(1334-1791)-His_6 was expressed in *Escherichia coli* strain BL21(DE3), affinity purified using Talon Metal Affinity Column (Clontech), and incubated with or without 20 ng of the purified CED-3 protease in the CED-3 buffer (50 mM Tris-HCl pH 8.0, 0.5 mM EDTA, 0.5 mM sucrose, 5% glycerol) at 30ºC overnight (*S6*). The samples were resolved by 15% SDS polyacrylamide gel (SDS-PAGE) and transferred onto PVDF membrane for amino terminal sequencing analysis. GST-DCR-1, GST-DCR-1(D1472E), GST-DCR-1(1472TEV)**,** GST-DCR-1(E1E2), and GST-DCR-1(E1D1E2) were

synthesized using the TNT Transcription/Translation coupled system (Promega) in the presence of both Methionine and ^{35}S-Methionine (50:1) and purified using Glutathione Sepharose beads (Promega). To express tDCR-1-FLAG and tDCR-1(del)-FLAG in *C. elegans*, transgenic animals carrying P_{hsp}tDCR-1-FLAG or P_{hsp}tDCR-1(del)-FLAG were grown in liquid culture at 20ºC for 5 days and then heat shocked at 33ºC for one hour. After six additional hours growing at 20ºC, the animals were harvested by 700 g centrifugation at 4ºC and washed three times with 150 mM KCl. Bacteria and fungi were removed by sucrose gradient centrifugation. The animals were then lysed by sonication in a buffer containing 25mM HEPES (pH 7.4), 150mM KCL, 10% Glycerol, 1 mM DTT, and 0.1 mM EDTA. The supernatant was collected by 14,000 g centrifugation at 4ºC for 30 minutes. tDCR-1-FLAG and tDCR-1(del)-FLAG were then affinity purified using anti-FLAG affinity column (Sigma) and eluted using 50 μM FLAG peptides as described previously (*S6)*.

CED-3 and TEV protease assays

CED-3 protease assays were done as described previously (*S6*). Briefly, GST-DCR-1, GST-DCR-1(D1472E), and GST-DCR-1(1472TEV) were synthesized and labeled with ^{35}S-Methionine using TNT Transcription/Translation coupled system (Promega) and incubated with 5 ng of purified CED-3 or 5 units of acTEV (Invitrogen) at 30ºC for 1 hour. The reactions were then resolved by 12% SDS-PAGE.

Plasmid cleavage assay and TdT assay

For the DNase activity assay, purified GST-DCR-1, GST-DCR-1(D1472E), GST-DCR-1(E1E2), GST-DCR-1(E1D1E2), GST-DCR-1(1472TEV), tDCR-1-FLAG, or tDCR-1(del)-FLAG was incubated with 200 ng of the supercoiled plasmid DNA in a buffer containing 20 mM HEPES-KOH (pH7.5), 3 mM $MgCl_2$, 10 mM KCl and 0.5 mM DTT at 37°C for 1 hour, in the presence or absence of 5 ng of purified CED-3. One half of the DNA samples were resolved on 1% agarose gel and then stained with ethidium bromide before a UV image was taken. The remaining half of DNA samples were then labeled with Terminal Deoxynucleotidyl Transferase (TdT) in a reaction buffer containing 20 mM Tris-acetate, 50 mM KOAc, 10 mM $MgOAc_2$, 250 μM $CoCl_2$, α-^{32}P dCTP at 37°C for 2 hours. The samples were resolved on 1% agarose gel, fixed and dried for autoradiography. For all agarose gels, 1 Kb Plus DNA ladder (Invitrogen) was used as DNA size markers.

DCR-1 ribonuclease assay

^{32}P labeled 189 bp dsRNA was synthesized by T7 RNA polymerase using the plasmid pPD129.36 that contains two T7 promoters in opposite orientation as a template. Fly Dicer-2, GST-DCR-1, GST-DCR-1(E1E2), and GST-DCR-1(E1D1E2) were incubated with the labeled dsRNA in a reaction buffer containing 20 mM HEPES-KOH (pH7.5), 3 mM $MgCl_2$, 10 mM KCl and 0.5 mM DTT at 37°C for 2 hours, in the presence or absence of 5 ng purified CED-3. The samples were resolved by 20% native polyacrylamide gel electrophoresis and stained with Ethidium Bromide. Image of siRNA ladder (New England Biolabs) was taken first and the polyacrylamide gel was then fixed and dried for autoradiography.

Protein amino terminal sequencing

Approximately 5 μg of DCR-1(1334-1791)-His_6 were incubated with 20 ng of purified CED-3 at 30°C overnight, resolved on 15% SDS-PAGE, transferred onto a PVDF membrane, and stained by Coomassie Brilliant Blue R-250. The cleavage products were then excised from the PVDF membrane and subjected to amino terminal sequencing (Tufts University Core Facility).

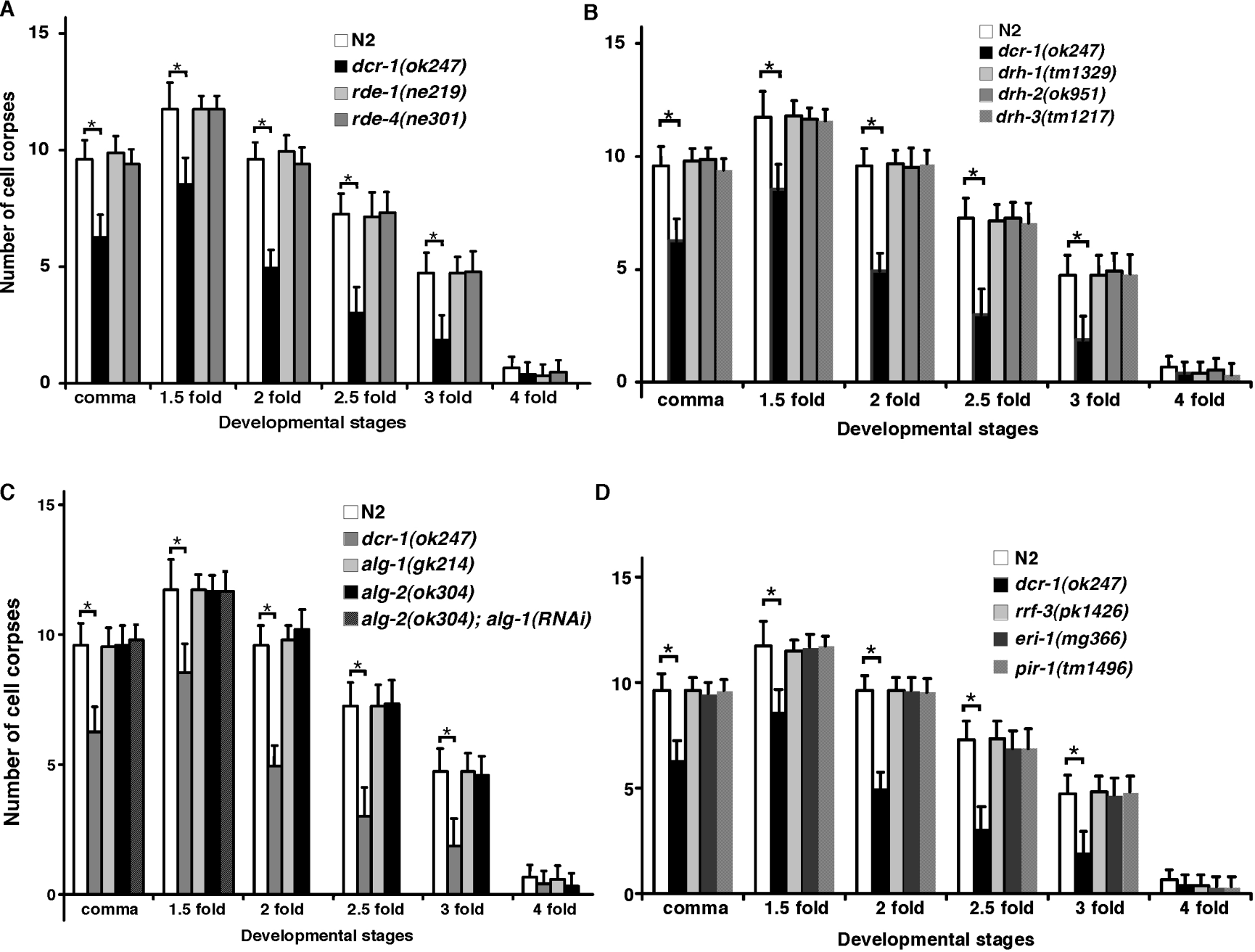

Figure S1. Analysis of embryonic cell deaths in animals deficient in DCR-1 co-factors. Cell corpses were scored in the following animals: (**A**) N2, *dcr-1(ok247)*, *rde1(ne219)* and *rde-4(ne301)* animals, (**B**) N2, *dcr-1(ok247)*, *drh-1(tm1329)*, *drh-2(ok951)* and *drh-3(tm1217)* animals, (**C**) N2, *dcr-1(ok247)*, *alg-1(gk214)*, *alg-2(ok304)* and *alg-2(ok304); alg-1(RNAi)* animals, (**D**) N2, *dcr-1(ok247)*, *rrf-3(pk1426)*, *eri-1(mg366)* and *pir-1(tm1496)* animals. Stages of embryos examined were: comma, 1.5-fold, 2-fold, 2.5-fold, 3-fold and 4-fold. Although *alg-1* RNAi treatment of the *alg-2(ok304)* mutant causes embryonic lethality, we could analyze embryos at the comma and 1.5 fold stages when they are still alive. The y axis represents average number of cell corpses scored and error bars are S.D. 15 embryos were counted for each developmental stage. The significance of differences between different genetic backgrounds was determined by two-way ANOVA, followed by Bonferroni comparison. *, $P < 0.001$; **, $P < 0.05$. All other points had P values > 0.05.

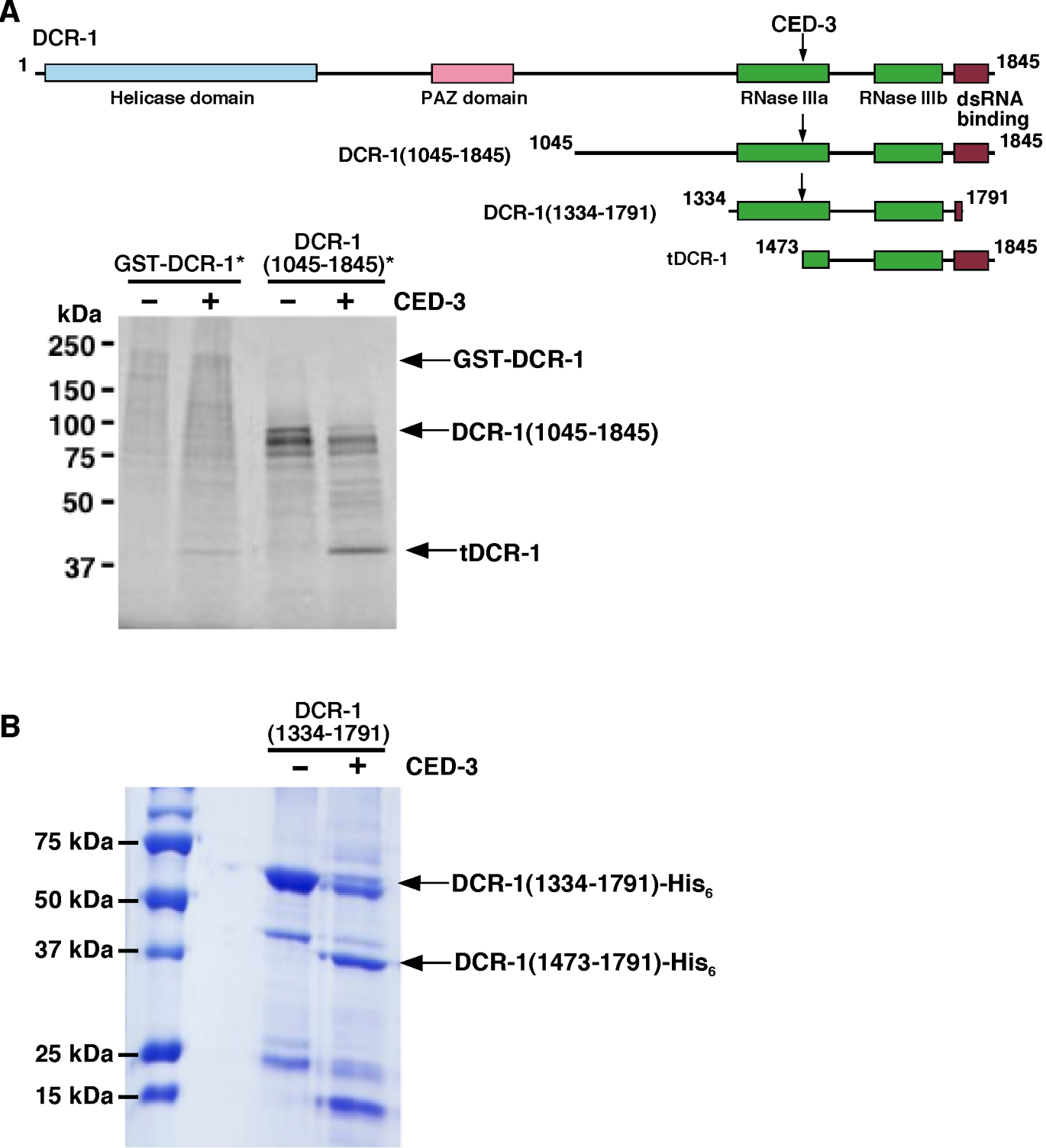

Figure S2. DCR-1 is cleaved by CED-3 at Asp 1472. (**A**) Upper panel, a schematic diagram of DCR-1, DCR-1(1045-1845), DCR-1(1334-1791), tDCR-1, and various DCR-1 domains. The CED-3 cleavage site is indicated with an arrow. Bottom panel, GST-DCR-1 and DCR-1(1045-1845)-His_6 were synthesized in rabbit reticulocyte lysate and labeled with ^{35}S-Methionine. They were then incubated with or without 5 ng of purified CED-3 for 1 hour at 30^{o}C and resolved by 12% SDS-PAGE. Autoradiography image is shown. (**B**) Amino terminal sequencing analysis of DCR-1 cleavage products. Approximately 5 μg of DCR-1(1334-1791)-His_6 were incubated with 20 ng of purified CED-3 at 30^{o}C overnight and resolved by 15% SDS-PAGE. The gel was then stained by Coomassie Blue. The 37 kDa protein band in the CED-3 (+) lane was subjected to amino terminal sequencing analysis as described in Materials and Methods.

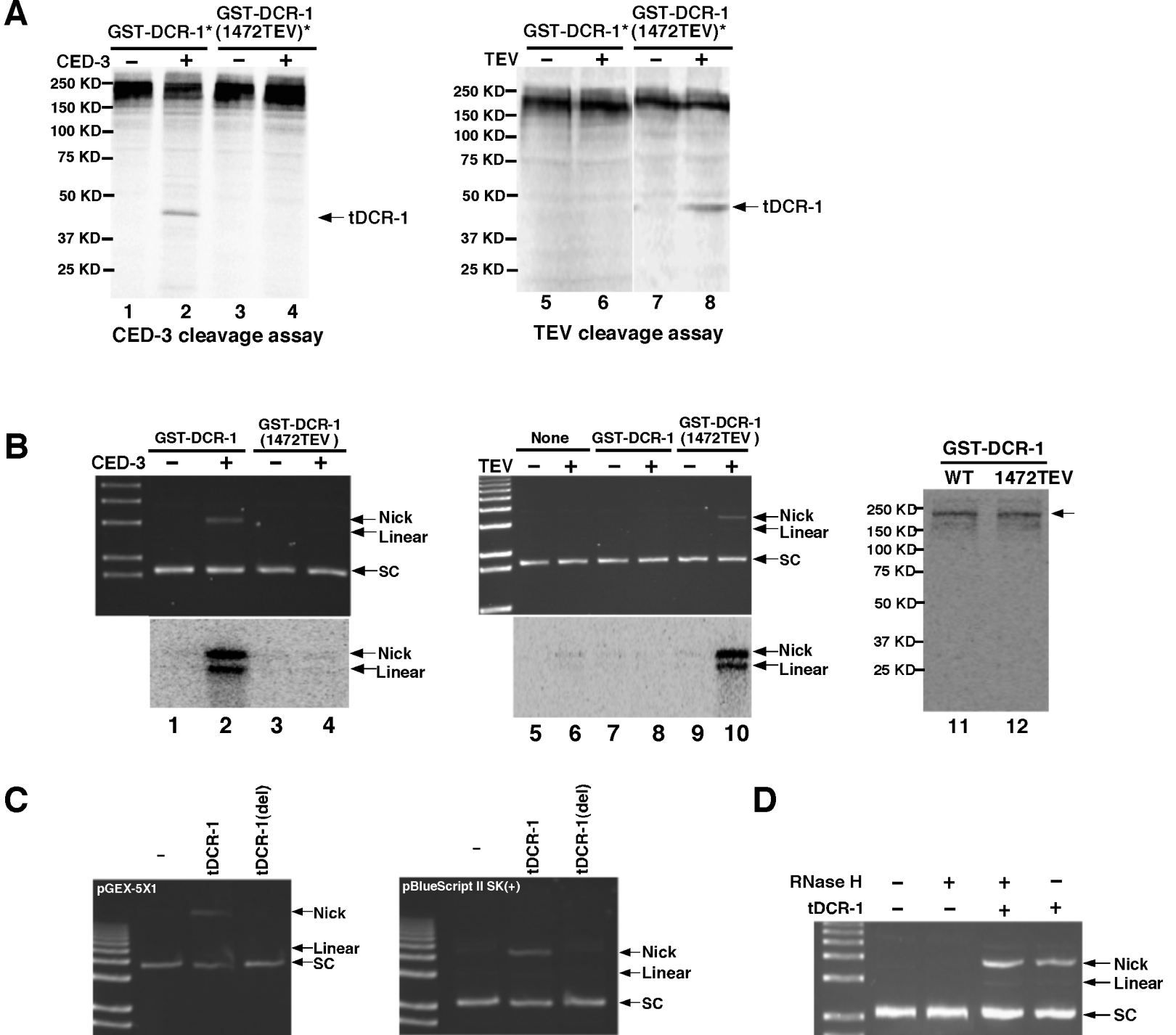

Figure S3. CED-3-activated DNase activity of DCR-1. (**A**) TEV but not CED-3 can cleave DCR-1(1472TEV), in which Asp 1472 of DCR-1 was replaced by a TEV cleavage site, to generate tDCR-1. GST-DCR-1 and GST-DCR-1(1472TEV) were synthesized in rabbit reticulocyte lysate and labeled with ^{35}S-Methionine. They were incubated with or without 5 units of acTEV (Invitrogen) or 2.5 ng of purified CED-3 for 1 hour at 30°C and resolved by 12% SDS-PAGE. (**B**) TEV but not CED-3 can activate a DNase activity from DCR-1(1472TEV). GST-DCR-1 and GST-DCR-1(1472TEV) were synthesized and purified as described in Fig. 3B and shown in lanes 11 and 12. They were incubated with or without 5 units of acTEV or 5 ng of purified CED-3 for one hour at 37°C and then with pUC19 plasmid DNA (200 ng) for another 1 hour at 37°C. TdT labeling was done as described in Fig. 3B. (**C**) Additional tDCR-1 DNase nicking assays. The nuclease activity assay and TdT labeling were done as in Fig. 3C with pGEX-5X1 and pBuleScript II SK(+), respectively. (**D**) RNase H does not nick or cleave supercoiled DNA. The nuclease activity assay was done as in Fig. 3C with pUC19. 1 unit of RNase H (Invitrogen) was used. In lane 3, RNase H and pUC19 were first incubated at 37°C for one hour and tDCR-1 was then added to the reaction and incubated for one additional hour.

Table S1. *dcr-1* acts in the same pathway as *cps-6* and *crn-2* to promote cell death and DNA degradation. All *cps-6(sm116)* strains also contain *dpy-5(e61)*. Extra cells were scored in the anterior pharynx of L4 hermaphrodites using Nomarski optics as described in Materials and Methods. 20 animals were scored for each strain. Data shown are mean ± s.e.m. The significance of difference between extra cell numbers derived from different genetic backgrounds was determined by one-way ANOVA, followed by Tukey's test. *dcr-1(ok247); ced-3(n2438)* or *dcr-1(pk1351); ced-3(n2438)* compared with *ced-3(n2438)*: $P < 0.001$. *ced-3(n2438); crn-2(tm1177)* or *cps-6(sm116); ced-3(n2438)* compared with *ced-3(n2438)*: $P < 0.05$.

Genotype	No. of extra cells	Range
N2	0.1 ± 0.1	0-1
dcr-1(ok247)	0.4 ± 0.1	0-1
dcr-1(pk1351)	0.4 ± 0.1	0-1
ced-3(n2438)	1.3 ± 0.3	0-3
dcr-1(ok247); ced-3(n2438)	3.1 ± 0.3	1-5
dcr-1(pk1351); ced-3(n2438)	3.1 ± 0.3	1-5
crn-2(tm1177)	0.2 ± 0.1	0-1
ced-3(n2438); crn-2(tm1177)	2.7 ± 0.3	1-5
dcr-1(ok247); ced-3(n2438); crn-2(tm1177)	2.8 ± 0.3	1-5
cps-6(sm116)	0.1 ± 0.1	0-1
cps-6(sm116); ced-3(n2438)	2.9 ± 0.3	1-6
cps-6(sm116); dcr-1(ok247); ced-3(n2438)	2.9 ± 0.3	1-5

Table S2. Loss of *dcr-1* co-factors does not affect the number of TUNEL-stained cells in the *cps-6(sm116)* mutant. All *cps-6(sm116)* strains also contain *dpy-5(e61)*. TUNEL staining was done as described in Fig. 1. 15 comma stage embryos were scored for each strain. Data shown are mean ± s.e.m. Although *alg-1*(RNAi) treatment of the *alg-2(ok304)* mutant causes embryonic lethality, we could analyze embryos at comma stage, since those embryos were still alive at comma and 1.5-fold stage.

Genotype	No. of TUNEL
N2	3.8 ± 0.63
cps-6(sm116)	16 ± 0.75
cps-6(sm116); dcr-1(ok247)	3.3 ± 0.58
cps-6(sm116); rde-1(ne219)	18 ± 1.0
cps-6(sm116); rde-4(ne301)	18 ± 0.76
cps-6(sm116); drh-1(tm1329)	16 ± 0.70
cps-6(sm116); drh-2(ok951)	19 ± 0.61
cps-6(sm116); alg-1(gk214)	19 ± 0.62
cps-6(sm116); alg-2(ok304)	18 ± 1.0
cps-6(sm116); alg-1(RNAi)	17 ± 1.0
cps-6(sm116); alg-2(ok304); alg-1(RNAi)	18 ± 0.77
cps-6(sm116); rrf-3(pk1426)	16 ± 0.71
cps-6(RNAi)	16 ± 0.72
drh-3(tm1217); cps-6(RNAi)	16 ± 0.77
eri-1(mg366); cps-6(RNAi)	17 ± 0.90
pir-1(tm1496); cps-6(RNAi)	15 ± 0.74

Table S3. Rescue of the vulva defects of *dcr-1(ok247)* animals by expression of various DCR-1 mutants. Vulva defects were scored in adult hermaphrodites using Nomarski optics. Each numbered array represents an independent transgenic line. 50 animals were scored for each strain.

Genotype	Array	% vulval defects
N2		2
dcr-1(ok247)		60
dcr-1(ok247); ex[P_{dcr-1}DCR-1]	1	16
	2	6
	3	8
dcr-1(ok247); ex[P_{dcr-1}DCR-1(D1472E)]	1	10
	2	16
	3	8
dcr-1(ok247); ex[P_{dcr-1}tDCR-1]	1	62
	2	54
	3	66
dcr-1(ok247); ex[P_{dcr-1}DCR-1(E1E2)]	1	20
	2	20
	3	24
dcr-1(ok247); ex[P_{dcr-1}DCR-1(E1D1E2)]	1	58
	2	66
	3	62

Table S4. tDCR-1 overexpression did not induce cell death in the *ced-3(n2433)* mutant. Two independent P_{hsp}tDCR-1 or P_{hsp}tDCR-1(del) transgenic arrays described in Fig. 4F and 4G were crossed into the *ced-3(n2433)* mutant and subjected to heat-shock treatment as described in Materials and Methods. Cell corpses were scored using Nomarski optics. 15 embryos were scored for each embryonic stage. Stages of embryos scored were: comma, 2-fold, and 4-fold. Data shown are mean ± standard deviation (S.D.).

Genotype	No. of cell corpses		
	Comma	2-fold	4-fold
ced-3(n2433)	0 ± 0	0 ± 0	0 ± 0
ced-3(n2433); ex[P_{hsp}tDCR-1]#1	0 ± 0	0 ± 0	0 ± 0
ced-3(n2433); ex[P_{hsp}tDCR-1]#2	0 ± 0	0 ± 0	0 ± 0
ced-3(n2433); ex[P_{hsp}tDCR-1(del)]#1	0 ± 0	0 ± 0	0 ± 0
ced-3(n2433); ex[P_{hsp}tDCR-1(del)]#2	0 ± 0	0 ± 0	0 ± 0

References and Notes

S1. S. Brenner, *Genetics* **77**, 71 (1974).
S2. J. Parrish *et al.*, *Nature* **412**, 90 (2001).
S3. C. C. Mello, J. M. Kramer, D. Stinchcomb, V. Ambros, *EMBO J*. **10**, 3959 (1991).
S4. T. Gu, S. Orita, M. Han, *Mol. Cell Biol.* **18**, 4556 (1998).
S5. H. Tabara *et al.*, *Cell* **99**, 123 (1999).
S6. D. Xue, S. Shaham, H. R. Horvitz, *Genes Dev.* **10**, 1073 (1996).